ACTA ORTHOPAEDICA et TRAUMATOLOGICA TURCICA
www.aott.org.tr

Research Article

Effect of kirenol on the interaction between the WNT/β-Catenin and RUNX2/TCF/LEF1 pathways in fracture healing *in vivo*

İbrahim Karaman[1], Ali Eray Günay[2], Mükerrem Betül Yerer[3], Eren Demirpolat[3], Serap Doğan[4], Arzu Hanım Yay[5], İbrahim Halil Kafadar[1]

[1]*Department of Orthopedics and Traumatology, Erciyes University, School of Medicine, Kayseri, Turkey*
[2]*Clinic of Orthopedics and Traumatology, Kayseri City Hospital, Kayseri, Turkey*
[3]*Department of Pharmacology, Erciyes University, School of Pharmacy, Kayseri, Turkey*
[4]*Department of Radiology, Erciyes University, School of Medicine, Kayseri, Turkey*
[5]*Department of Histology, Erciyes University, School of Medicine, Kayseri, Turkey*

ARTICLE INFO

Article history:
Submitted 7 December 2018
Received in revised form
30 March 2019
Last revision received
18 January 2020
Accepted 09 February 2020

Keywords:
Herba Siegesbeckia
Kirenol
Wingless Type
β-Catenin
rhBMP-2

ORCID iDs of the authors:
İ.K. 0000-0002-0347-9622,
A.E.G. 0000-0002-3496-1155,
M.B.Y. 0000-0002-4503-8032,
E.D. 0000-0003-4405-4660,
S.D. 0000-0001-6331-2245,
A.H.Y. 0000-0002-0541-8372,
İ.H.K. 0000-0001-7382-0702.

ABSTRACT

Objective: This study aimed to determine the effects of a natural diterpenoid, kirenol, on fracture healing in vivo in an experimental rat model of femur fracture and investigate its potential mechanism of action via the Wnt/β-catenin pathway.

Methods: In this study, 64 male Wistar albino rats aged 5-7 weeks and weighing 261–348 g were randomly divided into 8 groups from A to L, with eight rats in each group. Standardized fractures were created in the right femurs of the rats and then fixed with an intramedullary Kirschner wire. Four experimental groups were administered 2 mg/kg/day kirenol (Groups C and G) and 4 mg/kg/day (Groups D and H) kirenol by oral gavage.Thereafter, the animals were sacrificed at two time points as follows: on the 10th day (Groups B, C and D) and on the 21st day (Groups F, G and H) after the surgery; fracture healing in each group was assessed radiologically and histopathologically. The Radiographic Union scale of tibia fracture scoring system was used in the radiological examination; callus volume and density were measured using computed tomography. In the histopathologic examination, the scoring system described by Huo et al. was used. Additionally, the mechanism of action was evaluated based on the analyses of protein expression of Wnt3a, LRP5, TCF-LEF1, β-catenin, and Runx-2 proteins using western blot analysis.

Results: Among the animals sacrificed on the 10th day after the surgery, the highest histopathological and radiological scores were observed in Group D ($p<0.05$). Furthermore, the callus density ($p<0.05$) was highest in Group D. Among the animals sacrificed on the 21st day, the highest histopathological and radiological scores were found in Group H, although the differences among the groups were not significant ($p>0.05$). The callus volume and density were the highest in Groups G and H, respectively, although the differences among groups were not significant.

Conclusion: Kirenol may improve fracture healing in a dose-dependent manner with the early activation of the Wnt/β-catenin pathway and the activation of the Runx-2 pathway.

Introduction

Despite improvements in the regeneration and repair capacities of bones and the related treatments, healing is challenging in approximately 5%–10% of all fractures (1). Nonunion and delayed unions are important complications for both the patient and the clinician and often require long-term treatment. The etiologies of nonunion and delayed union remain unclear; however, both systemic and local factors are believed to influence these processes (2).

Wingless type (Wnt) is a glycoprotein that was first isolated in 1982 from the breast tissue of rats with cancer, and it comprises 19 sub-types (3). The canonical pathway is activated by the binding of Wnt to the "Frizzled transmembrane receptor" and the low-density lipoprotein receptor related peptides (LRP) 5 and 6 co-receptors (4). Binding of Wnt to these receptors increases the cell β-catenin levels by inactivation of the catenin destruction complex (5). β-catenin binds "T cell factor/lymphoid enhancer factor1" (TCF/LEF1),

Corresponding Author:
İbrahim Karaman
drikaraman@gmail.com

Content of this journal is licensed under a Creative Commons Attribution-NonCommercial 4.0 International License.

Cite this article as: *Karaman İ, Günay AE, Yerer MB, et al. Effect of kirenol on the interaction between the WNT/β-Catenin and RUNX2/TCF/LEF1 pathways in fracture healing in vivo. Acta Orthop Traumatol Turc 2020; 54(3): 320-9. DOI: 10.5152/j.aott.2020.03.529.*

DOI: 10.5152/j.aott.2020.03.529

causing a twist in the DNA and allows the transcription of Wnt target genes (6). In addition to the activation of the canonical pathway, Wnt3a induces osteoblast differentiation and suppresses apoptosis (7). Runt-related transcription factor-2 (Runx-2) is indispensable for endochondral bone development with bone morphogenetic protein (BMP) (8). It plays an important role in osteoblast differentiation and skeletal development (9).

Kirenol is a diterpenoid derived from the Herba Siegesbeckiaplant (10). Herba Siegesbeckia is a historical, tropical plant that is used for treating arthritis, malaria, hypertension, and snakebites in China (11). Kirenol decreases the activation of IL-1β, TNF-α, NF-κB, IL-6, and B-cell lymphoma 2 (Bcl-2); activates annexin-1, IL-2, BMP, and Wnt pathways; increases LRP-5 and β-catenin mRNA expression; and inhibits β-catenin-phosphorylating glycogen synthase kinase 3 beta (GSK3β). Thus, kirenol exerts anti-inflammatory, antiadipogenic, immunoregulatory, antioxidant, and antiarthritic effects (11-17).

Table 1. Naming of the groups and number of rats

	Hour 0	Day 10	Day 21	Healthy
Control	Group A n=8	Group B n=8	Group F n=7	Group L n=8
Kirenol 2 mg/kg		Group C n=8	Group G n=8	
Kirenol 4 mg/kg		Group D n=8	Group H n=8	

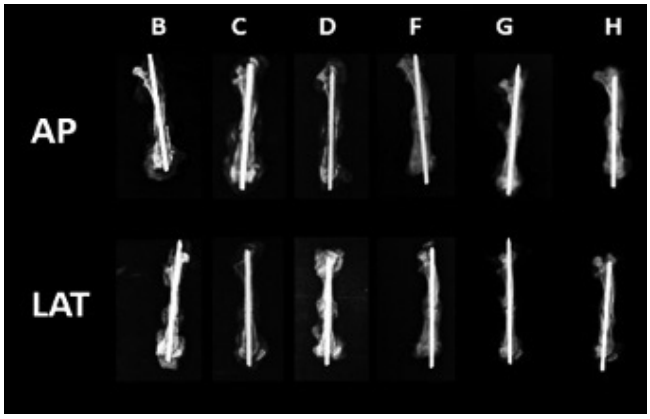

Figure 1. Anterior posterior (AP) and lateral (LAT) x-ray images of one subject from each group

HIGHLIGHTS

- Kirenol affects femoral fracture union positively.
- The effect of kirenol increases with dosage.
- Kirenol shows its positive effect on fracture healing by activating the Wnt / β-Catenin pathway and Runx2 on early period.

In the present study, the effects of kirenol on the healing of experimentally induced femur bone fracture and its possible mechanism of action via the "Wnt/β-catenin" pathway were investigated.

Materials and Methods

Experimental animals

In this study, 64 male Wistar albino rats with an average weight of 308.3±21.5 g (261–348 g) aged 6 (5–7) months were used. The rats were exposed to a light/dark cycle of 10/14 h, kept at normal room temperature, and fed standard mouse diet and tap water.

Kirenol procurement

We obtained 1.25 mg of 99% pure kirenol (TRC-K570300) from Toronto Research Chemicals (Canada) that was maintained at cold temperatures throughout the study.

Surgical interventions

The rats were randomly divided into eight groups of eight rats each (Table 1). Under general anesthesia, the right lower extremities of all rats were prepared under sterile conditions, fractures were induced in the right femurs in 56 rats (Group A, B, C, D, F, G, H), and intramedullary fixation was performed using a 1.5-mm Kirschner (K) wire in 48 rats (Group B, C, D, F, G, H).

The femoral bones of eight rats in Group L were removed without inducing fracture. Eight rats in Group A were sacrificed without any procedures 1 h after inducing fracture, and their femur bones were removed.

2 mg/kg kirenol was mixed with and dissolved in DMSO at a ratio of 2:100 and then diluted to a ratio of 1:10 in SF and administered via oral gavage to 16 rats in Groups C and G starting on day 1 after the fracture.

4 mg/kg kirenol was mixed with and dissolved in DMSO at a ratio of 1:100 and then diluted to a ratio of 1:10 in SF and administered via oral gavage to 16 rats in Groups D and H starting from day 1 after the fracture.

Starting from day 1 after fracture induction, 0.04 mg/kg of DMSO diluted to a ratio of 1:10 in SF was administered daily via oral gavage to 16 rats in Groups B and F, which constituted the control groups.

One rat in the group F was excluded from the study because he died.

After being administered anesthesia, the rats were kept in separate environments during the recovery period and placed at the Erciyes University experimental research and application center. All the rats were sacrificed using intracardiac potassi-

um injection. After the sacrifices, the femurs of the rats were removed from the surrounding soft tissue while preserving the callus tissue and sent for further experiments as follows.

All procedures were performed in accordance with the United Kingdom Animal Act (Scientific Procedures) 1986 and the relevant guidelines.

Radiographic evaluation

To obtain radiographs, the specimens were placed on the radiography cassette according to group and sequence numbers (Siemens©, Multix C). AP and lateral images were evaluated according to the Radiographic Union scale of tibia fracture (RUST) scoring system (Figure 1) (18). Each cortex of the femur (medial, lateral, anterior, and posterior) was scored out of 3 and summed. Measurements were performed twice each by three authors. The mean of the six measurements were recorded as the radiological results.

Computed tomography (CT)

CT images (Toshiba Aquilion One©, Japan) were obtained at a thickness of 0.5 mm from the removed femurs. The single-energy metal artifact reduction technique was used to reduce the metal artifacts in the images; the callus volume (mm^3) was calculated on the images taken to the tomography workstation (Vitrea, Toshiba Medical Systems) (Figure 2).

The region of interest covering only the callus was then plotted in the section with the most distinct callus tissue, and density was measured according to the Hounsfield scale (air=−1000, water=0, and bone=+1000).

Histopathological examination

After the radiological examination, the fracture line was initially cut transversely 5-mm proximally and distally using a diamond-tipped saw (Exakt 300 CL, Exakt® Apparatbau, Norderstad, Germany) connected to a precision cutting device and then sagittally divided into two equal pieces.

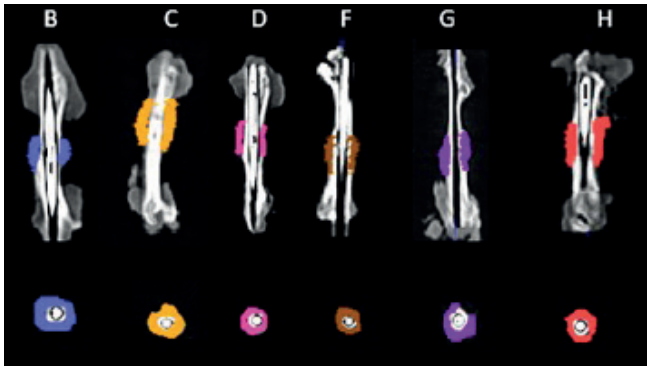

Figure 2. Coronal and axial CT-CV images of one subject from each group

Region of Interest covering only the callus was then plotted in the section with the most distinct callus tissue and density was measured according to Hounsfield Score (Air = −1000, Water = 0, Bone = +1000)

The lateral piece was reserved for western blotting, and the medial piece was reserved for histopathological examination. Harvested bone tissues were fixed in 10% formalin solution for 1 week. The samples were decalcified in 10% EDTA in phosphate-buffered saline (pH 7.4) and were dehydrated in graded ethanol solutions (70%–100%) and xylene before embedding in paraffin. From the paraffin-embedded samples, 5-µm sections were placed on poly-L-lysine slides. Images at 10x and 20x magnifications were captured using an Olympus BX-51 light microscope (Olympus BX-51, Tokyo, Japan) equipped with a digital camera. Masson's triple staining was performed for histopathological examination of fracture healing according to the scoring system described by Huo et al. (19).

Western Blot Analysis

Preparation of protein isolation solution

The protein isolation solution was prepared using radioimmunoprecipitation assay (RIPA) lysis buffer and protease inhibitors. One EDTA-free Roche complete mini protease inhibitor cocktail (Roche 11836157001) tablet was used for every 10 mL of the lysis buffer, and other protease inhibitors, such as phenylmethylsulphonyl (Sigma P7626), aprotinin (Applichem A2132), leupeptin (Applichem A2183), and pepstatin A (Applichem A2205) were added to this cocktail.

Bone homogenization and protein extraction

Bone samples were taken from the −80°C refrigeration unit, weighed on a precision scale, and subjected to homogenization using 500 µL of protein isolation solution per 100 mg of bone tissue. RIPA lysis buffer (tris-HCl 50 mM, NaCl 150 mM, Triton 1%, SDS 0.1%, sodium deoxycholate 0.5%, and water solution) that contained a protease inhibitor cocktail (Roche 11836157001) and the inhibitors PMSF 1 mM, aprotinin 2 µg/mL, leupeptin 10 µg/mL, and pepstatin A 2 µg/mL was used for homogenization. Bone tissue was disintegrated using a homogenizer (IKA T25 Ultra Turrax) for 1 min in a cold environment with ice and sonicated (Bondelin Sonoplus HD 2070) and centrifuged (Thermoscientific SL 16R) at 15,000 rpm for 15 min at 4°C. The pellet containing cell debris was discarded, and the protein-containing supernatant was placed into clean Eppendorf tubes for determining the total protein concentration.

Measurement of the total protein concentration

The total protein concentration of the protein mixture obtained from the bone tissue was measured using the BCA protein assay kit (Thermoscientific 23225) via the bicinchoninic acid (BCA) method. Standard samples for analysis were prepared by dissolving bovine serum albumin (Sigma A2153) in distilled water at concentrations of 1, 2, 4, 8, and 16 µg/µL. The total protein levels of standard samples were measured, and the total protein levels were calculated from the absorbance data of unknown samples using the linear

Table 2. Comparison of the radiography scores of rats that were sacrificed on days 10 and 21. Data are shown as arithmetic mean±SD values and median (range) values. The difference between the groups was statistically significant (p<0.05)

	Day 10		
	B (n=8)	**C (n=8)**	**D (n=8)**
Radiography score	6.3±1.5[a] 6.6 (4.0–8.0)	7.2±1.6[a] 7.5 (4.0–8.8)	8.1±1.3[b] 8.3 (5.5–10.1)
Kruskal–Wallis	6.33		
p	**0.042**		
	Day 21		
	F (n=7)	**G (n=8)**	**H (n=8)**
X - Ray	8.0±0.7 8.0 (7.1–8.8)	8.0±1.1 8.3 (6.7–9.5)	8.6±0.4 8.0 (7.2–8.5)
Kruskal–Wallis	0.169		
p	0.919		

equation obtained from the absorbance versus concentration graph.

Western blot analysis

The levels of β-catenin, LRP5, Wnt3a, RUNX-2, TCF1, and LEF1 proteins in the Wnt3a pathway were examined, and GAPDH was used as a housekeeping protein. The experiments were performed using the Biorad mini protean tetra cell system. The polyacrylamide concentration of SDS-PAGE gels were 7% and 10% depending on the protein size. After separation, the proteins were transferred to polyvinylidene fluoride (PVDF) membranes (Bio Rad 162-01777). The membranes were blocked with 5% skim milk that was dissolved in Tris-buffered sodium solution containing 0.1% Tween 20 (TBS-T) for 1 h. Rabbit primary and goat anti-rabbit antibodies were used for detection and were dissolved in TBS-T. Proteins were visualized with a chemiluminescent substrate (Bioexpress Advansta E-1119-20) and detected using radiography (Thermoscientific 34090). The analyses were performed using Image J 1.50i software, and the proteins were normalized using a housekeeping protein GAPDH.

Table 3. Comparison of the callus volume (CT-CV) and callus density (CT-CD) results of rats that were sacrificed on days 10 and 21. Data are shown as arithmetic mean±SD values and median (range) values. The difference between the groups was statistically significant (p<0.05)

	Day 10		
Groups	**B (n=8)**	**C (n=8)**	**D (n=8)**
CT-CV	224.8±90.5 232.2 (99.9–385.9)	203.3±154.6 157.1 (53.9–526.9)	229.6±89.2 250.4 (30.7–317.2)
Kruskal–Wallis	0.96		
p	0.62		
CT-CD	−58.3±92.6 −35.7 (−190.1–61.3)	48.8±81.1 25.1 (−15.7–223.0)	44.8±48.3 41.3 (−36.7–129.5)
Kruskal–Wallis	5.95		
p	0.05		
	Day 21		
Groups	F (n=7)	G (n=8)	H (n=8)
CT-CV	158.3±87.2 140.0 (65.2–277.5)	225.3±126.2 243.9 (49.0–411.5)	209.1±67.5 185.3 (136.3–321.3)
Kruskal–Wallis	2.502		
p	0.286		
CT-CD	260.0±103.0 230.6 (147.0–411.3)	244.1±102.1 290.2 (103.9–379.1)	279.6±112.9 300.9 (161.3–444.0)
Kruskal–Wallis	0.394		
p	0.821		

Statistical analysis

Data were assessed using the Statistical Package for Social Sciences, version 22.0 (IBM Corp.; Armonk, NY, USA) software. The normal distribution of the quantitative data was assessed using the Shapiro–Wilk test; we found that the data were non-normally distributed. The CT-callus volume (CT-CV), CT-density (CT-D), histopathological score (HPS), and radiography score (RS) of the groups were compared using the Kruskal–Wallis (KW) test. Dunn test was used for identifying groups that caused the difference in cases where the difference was significant. Spearman correlation analysis was performed to evaluate the relationship between the variables. Quantitative data were expressed as mean±standard deviation (SD) values and median (range) values; $p<0.05$ was considered statistically significant in all analyses. For western blotting, statistical analysis was performed separately in the treatment (Group C, D, G, H) and non-treatment groups (Group A, B, F, L) using the T-test.

Results

Radiographic evaluation

The radiographs were scored using the RUST scoring system. The 10th-day and 21st-day groups were compared among themselves (Table 2).

Table 4. Comparison of the HPS results in rats sacrificed on days 10 and 21. Data are shown as arithmetic mean±SD values and median (range) values. The difference between the groups was statistically significant ($p<0.05$)

	Day 10		
	B (n=8)	**C (n=8)**	**D (n=8)**
Histopathological score	2.6±2.5[a] 2.0 (0–6)	5.9±0.8[b] 6.0 (4–7)	6.6±0.7[b] 6.5 (6–8)
Kruskal–Wallis	13.05		
p	**0.001**		
	Day 21		
	F (n=7)	**G (n=8)**	**H (n=8)**
Histopathological score	6.3±1.4 6.0 (5.0–8.0)	6.7±0.8 7.0 (6.0–8.0)	7.4±1.4 7.0 (6.0–9.0)
Kruskal–Wallis	2.50		
p	0.29		

Table 5. Spearman correlation analysis of the CT-CV, CT-CD, HPS, and RS values

	CT-CV	CT-CD	HPS
CT-CD	−0.197		
HPS	0.131	0.468**	
RS	−0.070	0.317*	0.412**

The mean RS of Group D was significantly higher than those of Groups B and C ($p<0.05$); the mean RS of Group H was higher than that of Groups F and G; however, the differences between the groups were not significant ($p>0.05$). Moreover, the mean RS of Group D was higher than that of the 21st-day control group (Group F); however, the difference between the groups was not significant ($p>0.05$). Thus, the mean RS of Groups D and H were higher than that of all the other groups.

CT evaluation

CT-CV and CT-CD measurements were performed using the CT images (Figure 2). The 10th-day and 21st-day groups were compared among themselves (Table 3).

In the 10th-day groups, the mean CT-CV of Group D was higher than that of Groups B and C; the mean CT-CD of Groups C and D was higher than that of group B. However, the differences were not significant ($p>0.05$). In the 21st-day

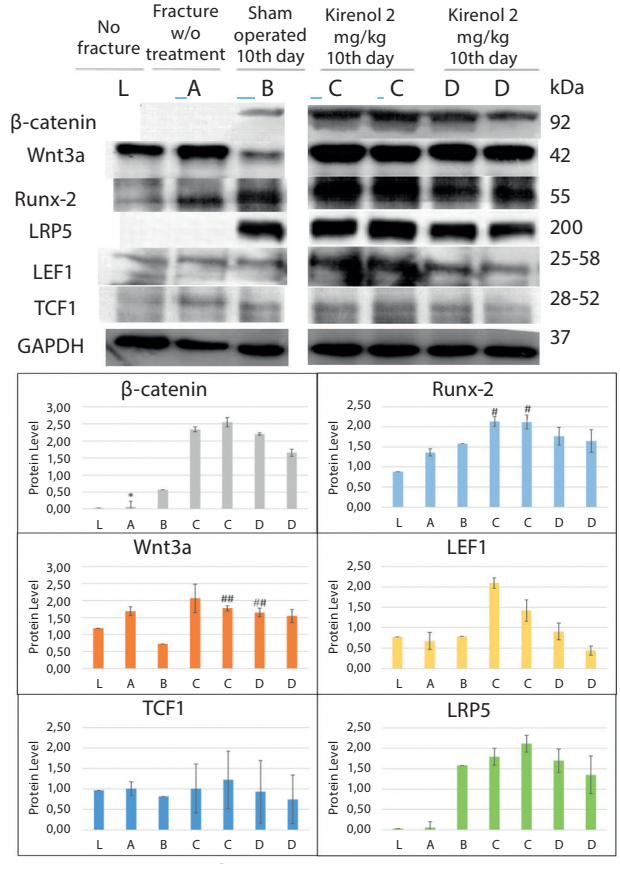

Figure 3. Graphs of Wnt3a, β-Catenin, LRP 5, Runx-2, TCF, and LEF Western Blotting results and Image j analysis in 10th day subjects

L: No fracture, A: Fracture w/o treatment, B: Fracture and 30μg C: Fracture and 2 mg/kg kirenol treatment, D: Fracture and 4 mg/kg kirenol treatment
Protein level resembles the image and standard deviation belongs to mean data. Statistical analysis performed using all replicates. t test, * or # $p<0,05$, ** or # # $p<0,001$. Statistical analysis performed in treatment and non treatment groups seperately. (L and A), (B to D)

groups, the mean CT-CV of Group G was higher than that of the other groups, and group H had the highest CT-CD mean value. However, the differences between the groups were not statistically significant (p>0.05).

Histopathological evaluation

The 10th-day and 21st-day groups were compared among themselves (Table 4). Among the 10th-day rats, the mean HPS of Group C and D was significantly higher than that of Group B (p< 0.05). Moreover, the mean HPS of Group D was higher than that of the 21st-day control group (Group F); however, the difference was not significant (p>0.05).

Among the 21st-day rats, the mean HPS of Groups G and H was higher than that of Group F; however, the difference was not statistically significant (p>0.05).

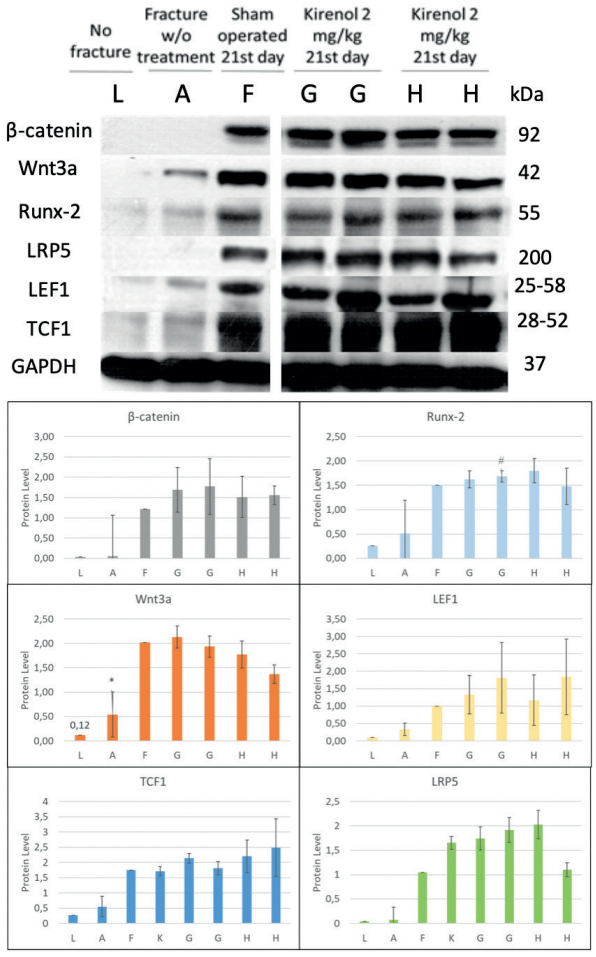

Figure 4. Graphs of Wnt3a, β-Catenin, LRP 5, Runx-2, TCF, and LEF Western Blotting results and Image j analysis in 21st day subjects

L: No fracture, A: Fracture w/o treatment, F: Fracture and G: Fracture and 2 mg/kg kirenol treatment, H: Fracture and 4 mg/kg kirenol treatment

Protein level resembles the image and standard deviation belongs to mean data. Statistical analysis performed using all replicates. T test, * or # p<0,05, ** or # # p<0,001. . Statistical analysis performed in treatment and non treatment groups seperately. (L and A), (F to H)

As noted in Table 2 and 4, the highest HPS (6.6±0.7) and RS (8.1±1.3) were obtained in the 10th day group that was administered kirenol at a dose of 4 mg/kg; the values were significantly different the 10th day sham operated group (group B) (p<0.05).

In the evaluation of the correlation between CT-CV, CT-CD, HPS, and RS of all groups, a correlation between histopathological evaluations and all other evaluation methods was observed; x-ray Scores were correlated with CT-CD and HPS (Table 5).

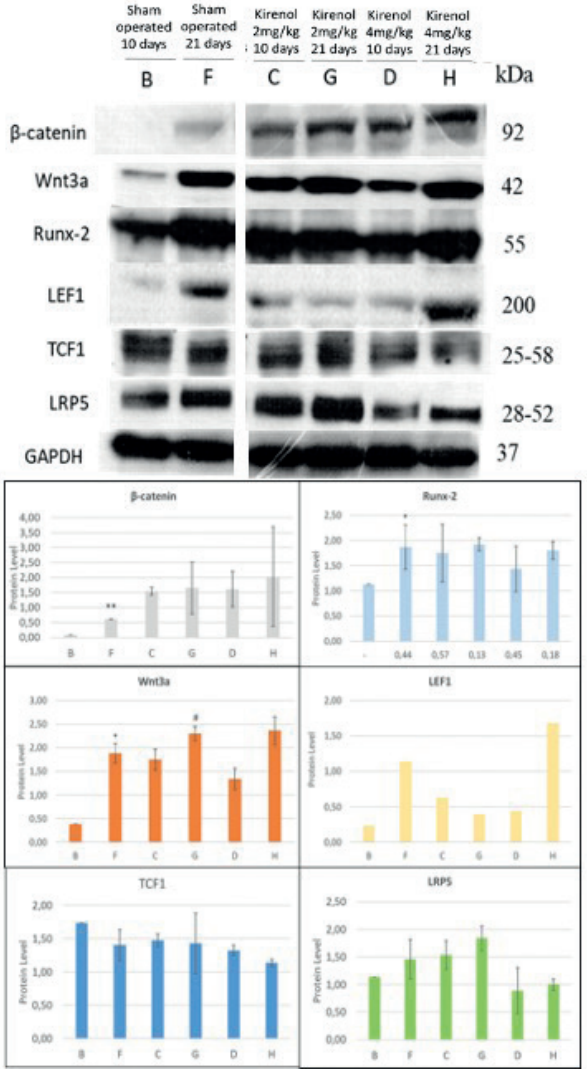

Figure 5. Graphs of Wnt3a, β-Catenin, LRP 5, Runx-2, TCF, and LEF Western Blotting results and Image j analysis in 10th and 21st day subjects

B: Fracture w/o treatment 10 days,
F: Fracture w/o treatment 21 days,
C: 2 mg/kg kirenol treatment 10 days,
G: 2 mg/kg kirenol treatment 21 days,
D: 4 mg/kg kirenol treatment 10 days,
H: 4 mg/kg kirenol treatment 21 days

Protein level resembles the image and standard deviation belongs to mean data. Statistical analysis performed using all replicates. t test, * or # p<0,05, ** or # # p<0,001. Statistical analysis performed in 10 days and 21 days groups seperately. (B,F), (C,G), (D,H)

Western blot analysis

Expression analysis of Wnt3a, β-catenin, Runx-2, LRP-5, TCF, and LEF1 proteins was performed using western blotting. After comparing the 10th-day and 21st-day groups among themselves, the ratio between the 0-h group (Group L without any fracture induced) and the 10th-day group as well as that between the 10th-day and 21st-day group was examined to determine the rate of increase in the protein expressions (Figure 3-6). The duration from 0 h to the 10th day was defined as the first period, and that from the 10th day to the 21st day was defined as the second period.

Increase in the expression was calculated in the first period using the ratio determined by the difference between the 10th day expression value of any groupwith Group Ldivided by that of Group L. E.g. [Group C increase= (Group C - Group L)/Group L].

Increase in the expression was determined in the second period by calculating the difference between the expression values on the 10th and 21st day in the groups treated using the same method and dividing the resultant value by the value obtained on the 10th day. E.g. [Group G increase= (Group G – Group C)/ Group C].

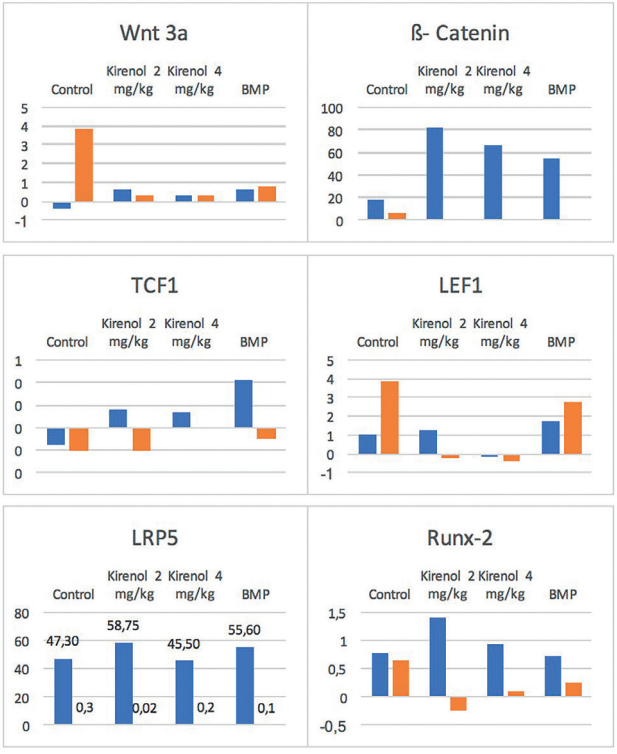

Figure 6. Daily change of Wnt3a, β-Catenin, LRP 5, Runx-2, TCF, and LEF Western Blotting levels according to the results obtained in Figure 3 and 5. Blue block shows the 1st Period, and orange block shows the 2nd Period

Wnt3a

Among the 10th-day groups, the highest Wnt3a level was observed in Group C ($p<0.001$), and Group D ($p<0.001$) had higher value than Groups A, B, and L (Figure 3, 5).

With respect to the 21st-day groups, the highest Wnt3a level was in Group G (Figure 4, 5).

In the first period, the Wnt3a expression increased by 30% in Groups C and D, while there was reduction in the expression in Group B. In the second period, Group F showed an increase that was 13-fold higher than that in Groups G and H (Figure 6).

β-catenin

Among the 10th-day groups, the highest β-catenin level was observed in Group C, and Group D had higher values than Groups A, B, and L (Figure 3, 5).

With respect to the 21st-day groups, the highest β-catenin level was observed in Group G, and Groups G and H had higher β-catenin expressions than Groups A, F, and L (Figure 4, 5).

In the first period, β-catenin expression increased 82-fold in Group C and 18-fold in Group B. In the second period, an increase of <1-fold was observed in Groups G and H, while Group F showed an increase of >8-fold compared with that in Group G (Figure 6).

Runx-2

Among the 10th-day groups, the highest Runx-2 expression was observed in Group C ($p<0.05$); Group D had higher values than Groups A, B, and L (Figure 3, 5).

In the 21st-day groups, the highest Runx-2 expression was observed in Group H ($p<0.05$); Groups F and G had similar Runx-2 expressions. In all these groups, Runx-2 expressions were higher than those in Groups A and L (Figure 4, 5).

In the first period, there was a 2-fold increase in Runx-2 expression in Group C compared with that in Group B, while the Runx-2 expression in Group C decreased during the second period (Figure 6).

LRP5

The highest LRP5 expression was observed in Group C among all the 10th-day groups; and Group D had higher values than Groups A, B, and L (Figure 3, 5).

The highest LRP5 expression was observed in Group H among the 21st-day groups; and Groups G and H had similar LRP5 expressions. In all these groups, the LRP5 expressions were higher than those in Groups A, F, and L (Figure 4, 5).

Similar changes were observed in the first and second periods in the control and 2 mg/kg–4 mg/kg kirenol groups (Figure 6).

TCF and LEF1

There was no consistent change in the levels of the intranuclear proteins TCF and LEF1 in the 10th-day groups (Figure 3, 5).

Among the 21st-day groups, Group H showed the highest TCF and LEF expressions; furthermore, the expressions of TCF and LEF in Group G were lower than those in Group H but higher than those in Groups A, F, and L (Figure 4, 5).

In addition, the 10th-day and 21st-day groups were compared with each other in terms of the adverse effects on Wnt3a, β-catenin, Runx2, LRP5, TCF, and LEF1; similar results were found using western blotting analysis (Figure 6).

Discussion

Our findings showed that kirenol improved fracture healing; this effect increased in a dose-dependent manner and was attributed to the early activation of the Wnt/β-catenin pathway and activation of the Runx-2 pathway.

The Wnt signaling pathway is believed to play an active role in bone healing and increase in bone mineral density. Baron et al. showed that the activation of the Wnt pathway increased bone strength and mineral density, and its inactivation was shown to increase bone fragility (20). Thus, an increasing number of studies are being conducted on the molecules that can activate this pathway for inducing bone healing. Kirenol, which has previously been shown to activate the Wnt pathways in osteoblast cultures, appears to be a suitable candidate for fracture healing (16). The activation of the Wnt pathway in the presence of a fracture was also supported by our western blot analyses of the control group and healthy rats. Experimentally induced femur fracture caused a minimal but acute increase in the levels of Wnt3a, an extracellular activator of the pathway, and its intracellular component β-catenin. Furthermore, the Wnt level was significantly higher in all groups compared with that in the group with healthy femur bones. This result supports the hypothesis that activation of the Wnt signaling pathway may occur as a response to the damage in the bone caused by the fracture, and the Wnt signaling pathway may contribute to bone repair.

Several researches have been conducted with the aim of accelerating fracture healing and minimizing the possibility of nonunion. In a cell culture study, Kim et al. showed that kirenol stimulated the canonical Wnt pathway that plays a key role in *in vitro* bone healing (16). In the present study, we investigated the *in vivo* effects of kirenol on fracture healing and the Wnt pathway and showed that fracture healing and the Wnt pathway were positively affected, especially in the early period of fracture healing. In agreement with our findings, Colburn et al. showed that post-fracture BMP administration activated fracture healing in the early period; however, this activation decreased in the later period (21). Horst et al. conducted a cell culture study and found that Wnt is activated in the early stages of fracture healing; however, it is inhibited by dickkopf related protein 1 (Dkk 1) for matrix calcification later in the healing process (22). In the present study, all experimental groups that were treated with kirenol had higher mean RH and HPS than the controls that were sacrificed on the same day. Although this difference was significant on the 10th day, the difference was non-significant on the 21st day. This was attributed to the fact that kirenol was able to accelerate the fracture healing process, and this process rapidly occurred during the first 10th days; however, as the process approached completion, the activation of fracture union was reduced and the recovery in the control group caught up with that in other groups, although it was initially delayed.

The rates of increase in Wnt3a, β-catenin, TCF, LRP 5, and Runx-2 expression in the 10th-day rats were higher in the kirenol groups than in the controls. In contrast, the rates of increase in Wnt3a, β-catenin, LEF, Runx-2, and LRP5 expression in the 10th–21th-day period were higher in the controls than in the kirenol groups. This finding supports the results of Horst (22), indicating that the Wnt/β-catenin pathway is more active during the early fracture healing process, these agents activate Wnt in the early period, and Wnt activity is subsequently reduced for calcification.

Although kirenol was locally administered in the study by Wang, Lua et al. investigated the antiarthritic effects of kirenol and administered kirenol by oral gavage at a dose of 2 mg/kg (12, 15). In the present study, kirenol was administered by the oral gavage route, and two different doses, 2 mg/kg and 4 mg/kg, were used for investigating the dose-dependent effects. The mean HPS and RS of the rats sacrificed on the 10th and 21st days were higher in the 4 mg/kg groups than in the 2 mg/kg groups. This suggests that kirenol achieves higher efficacy at increasing doses. However, these findings were not supported by the western blotting analysis findings. Consequently, higher RS and HPS were obtained in rats treated using 4 mg/kg kirenol; however, no absolute elevation in the protein expressions was detected.

The mean RS and HPS of fracture healing were not supported by western blot analysis for different doses of kirenol; however, Wnt3a, β-catenin, TCF-LEF, Runx-2, and LRP5 expressions on day 10 were higher in the kirenol groups than in the controls. This may be due to the higher dominant anti-inflammatory activity of kirenol at low doses, suppression of inflammatory processes owing to fracture healing, or because kirenol activates pathways other than the Wnt pathway.

The toxic dose of kirenol and its effects on various metabolic pathways at different doses should be investigated in future studies.

Kim et al. conducted a study in osteoblast culture wherein kirenol administration increased Wnt activation and induced matrix calcification (16). Therefore, the callus volume and density may be used as parameters to indicate fracture healing (18). Kirenol administration is expected to increase the callus volume and density. However, there was no significant difference among the callus volumes in the groups in the present study. This was attributed to the large SDs found in the intra-group callus means. This was caused by the lack of a rigid fixation method in the fixation process of fractures. In fractures that heal in a secondary manner, anatomic reduction and more stable fixation result in a better union and reduce the callus volume. Simultaneously, the callus volume can decrease in bones with poor reduction that fail to join (23). This means that the callus volume is not a direct indicator of the status of fracture healing. Although the callus volume is measured using radiographic methods, the callus density measured using CT appears to provide more consistent data (24, 25). In this study, there was a significant correlation between the HPS and RS results and the CT-D scores used in the evaluation of rats. Callus densities were increased in the 10th-day groups that were treated with 4 mg/kg kirenol. In this study, kirenol increased bone mineralization in the early period, which is consistent with the data in the literature.

Using western blotting analyses, we demonstrated that kirenol activates the Wnt signaling pathway. This activation may have been caused by the binding of kirenol to the LRP5 receptor and reduction in the intracellular active GSK3β protein levels or via direct inhibition of the activity of this enzyme.

Molecules that bind to the LRP5 and frizzled receptors in the Wnt signaling pathway are characterized by their lipid solubility and different chemical structures (26). On the basis of this, regardless of its molecular structure, kirenol could bind to Wnt receptors by dissolving in the cell membrane because of its lipophilic nature. In addition, kirenol increased the levels of LRP5 receptor measured in bone homogenate that may have been achieved via LRP5 located on the osteoblast cell surface. Based on this result, kirenol may also have increased total β-catenin levels and consequently increased LRP5 mRNA expression.

In addition to the effects on the Wnt signaling pathway, kirenol increased the Runx-2 levels. Via this effect, it may have contributed to bone healing by increasing the differentiation and proliferation of osteoblasts. Furthermore, the increase in β-catenin levels and the activation of the Wnt pathway may have contributed to the increase in the Runx-2 levels. A previous study has shown that Runx-2 and β-catenin increase the number, activity, and collagen synthesis of osteoblasts (27). This positive effect on bone synthesis through osteoblasts suggests that the Wnt signaling pathway and Runx-2 may be potential therapeutic targets for diseases in which bone mineral density and osteoclast activity increase, such as in osteoporosis. In fact, Kato et al. observed osteopenia in LRP5 knock-out Wnt signaling-inactive mice and concluded that LRP5 inactivation may be responsible for the osteoporosis-pseudoglioma syndrome that affects both the bone and the eye (28, 29). In the present study, the LRP5 levels increased more in the kirenol group than in the control group; furthermore, it activated the Wnt pathway by increasing the Wnt3a and β-catenin levels in addition to the LRP5 levels. Thus, kirenol may be beneficial in increasing mineral density in diseases characterized by bone loss, such as osteopenia and osteoporosis, owing to its effect on both Runx-2 and Wnt signaling pathway.

In conclusion, the possible effects of kirenol on fracture healing and the Wnt/β-catenin pathway in rats with experimentally induced femur fracture were investigated using radiological, histopathological, and metabolic data. It was shown that kirenol improved fracture healing; this effect increased as the dose increased. This effect of kirenol was caused by the early activation of the Wnt/β-catenin pathway and activation of the Runx-2 pathway. Therefore, we can conclude that kirenol is a herbal product, and future studies could investigate its effects on the human bone.

Ethics Committee Approval: Ethics committee approval was received for this study from the Clinical Ethics Committee of Erciyes University (approval date November 12, 2014; number 14/142).

Informed Consent: N/A.

Author Contributions: Concept - İ.K., A.E.G., M.B.Y.; Design - İ.K., A.E.G.; Materials - İ.K., A.E.G., E.D.; Data Collection and/or Processing – A.E.G., A.H.Y., S.D., E.D.; Analysis and/or Interpretation – İ.K., A.E.G., M.B.Y., E.D., S.D., A.H.Y., İ.H.K.; Writing Manuscript – İ.K., A.E.G., M.B.Y., E.D., S.D., A.H.Y., İ.H.K.

Conflict of Interest: The authors have no conflicts of interest to declare.

Financial Disclosure: This study was funded by TUBITAK (The Scientific and Technological Research Council of Turkey) as a part of 3001 initial research and development projects support program (Project number, 115s172) and Erciyes University Council of Scientific Investigations (Project Code TDA-2016-6136).

References

1. Einhorn TA. The cell and molecular biology of fracture healing. Clin Orthop 1998; 355: 7-21. [Crossref]
2. LaVelle DG. Delayed union and nonunion of fractures. In: Canale S.T. ed. Campbell's Operative Orthopaedics (10th ed), Philadelphia, Mosby Publishers. 2003; pp.3126.

3. Nusse R, Varmus HE. Many tumors induced by the mouse mammary tumor virus contain a provirus integrated in the same region of the host genome. Cell 1982; 3: 99-109. [Crossref]
4. He S, Lu Y, Liu X, et al. Wnt3a: functions and implications in cancer. Chin J Cancer 2015; 34: 554-62. [Crossref]
5. McDonald BT, Tamai K, He X. Wnt/β-catenin signaling: components, mechanisms, and diseases. Dev Cell 2009; 17: 9-26. [Crossref]
6. Nusse R, Varmus H. Three decades of Wnts: a personal perspective on how a scientific field developed. EMBO J 2012; 31: 2670-84. [Crossref]
7. Byun MR, Hwang JH, Kim AR, et al. Canonical Wnt signalling activates TAZ through PP1A during osteogenic differentiation. Cell Death Differ 2014; 21: 854-63. [Crossref]
8. Shu B, Zhang M, Xie R, et al. BMP2, but not BMP4, is crucial for chondrocyte proliferation and maturation during endochondral bone development. J Cell Sci 2011; 124: 3428-40. [Crossref]
9. Lian JB, Javed A, Zaidi SK, et al. Regulatory controls for osteoblast growth and differentiation: role of Runx/Cbfa/AML factors. Crit Rev Eukaryot Gene Expr 2014; 14: 1-4. [Crossref]
10. Xiao J, Yang R, Yang L, et al. Kirenol attenuates experimental autoimmune encephalomyelitis by ınhibiting differentiation of Th1 and Th17 cells and inducing apoptosis of effector T cells. Sci Rep 2015; 5: doi: 10.1038/srep09022. [Crossref]
11. Jiang Z, Yu QH, Cheng Y, Guo XJ. Simultaneous quantification of eight major constituents in Herba Siegesbeckiae by liquid chromatography coupled with electrospray ionization time-of-flight tandem mass spectrometry. J Pharm Biomed Anal 2011; 55: 452-7. [Crossref]
12. Wang JP, Zhou YM, Ye YJ, et al. Topical anti-inflammatory and analgesic activity of kirenol isolated from *Siegesbeckia orientalis*. J Ethnopharmacol 2011; 137: 1089-94. [Crossref]
13. Bi J, Xin HL, Lin ZF, et al. Effect of kirenol on cytokines in serum and apoptosis proteins expression in synoviocytes of adjuvant arthritis rats. Chinese Traditional and Herbal Drugs 2007; 38: 1207-10.
14. Kim MB, Song Y, Kim C, Hwang JK. Kirenol inhibits adipogenesis through activation of theWnt/β-catenin signaling pathway in T3-L1 adipocytes. Biochem Biophys Res Commun 2014; 445: 433-8. [Crossref]
15. Lua Y, Xiaob J, Wu ZW, et al. Kirenol exerts a potent anti-arthritic effect in collagen-induced arthritis by modifying the T cells balance. Phytomedicine 2012; 19: 882-9. [Crossref]
16. Kim MB, Song Y, Hwang JK. Kirenol stimulates osteoblast differentiation through activation of the BMP and Wnt/β-catenin signaling pathways in MC3T3-E1 cells. Fitoterapia 2014; 98: 59-65. [Crossref]
17. Qian RQ, Zhang CY, Fu HZ. Study on therapeutic mechanism of anti-rheumatism action of Herba siegesbeckiae. Chinese Journal of Integrated Traditional and Western Medicine 2002; 20: 192-5.
18. Augat P, Morgan EF, Lujan TJ, et al. Imaging techniques for the assessment of fracture repair. Injury 2014; 45: 16-22. [Crossref]
19. Huo MH, Troiano NW, Pelker RR, Gundberg CM, Friedlaender GE. The influence of ibuprofen on fracture repair: biomechanical, biochemical, histologic, and histomorphometric parameters in rats. J Orthop Res 1991; 9: 383-90. [Crossref]
20. Baron R, Kneissel M. WNT signaling in bone homeostasis and disease: from human mutations to treatments. Nat Med 2013; 19: 179-92. [Crossref]
21. Colburn NT, Zaal KJ, Wang F, Tuan RS. A role for gamma/delta T cells in a mouse model of fracture healing. Arthritis Rheum 2009; 60: 1694-703. [Crossref]
22. van der Horst G, van der Werf SM, Farih-Sips H, van Bezooijen RL, Löwik CW, Karperien M. Downregulation of Wnt signaling by increased expression of Dickkopf-1 and -2 is a prerequisite for late-stage osteoblast differentiation of KS483 cells. J Bone Miner Res 2005; 20: 1867-77. [Crossref]
23. Henderson CE, Lujan TJ, Kuhl LL, Bottlang M, Fitzpatrick DC, Marsh JL. Mid-America orthopaedic association physician in training award: healing complications are common after locked plating for distal femur fractures. Clin Orthop Relat Res 2011; 469: 1757-65. [Crossref]
24. Welch RD, Jones AL, Bucholz RW, et al. Effect of recombinant human bone morphogenetic protein-2 on fracture healing in a goat tibial fracture model. J Bone Miner Res 1998; 13: 1483-90. [Crossref]
25. Rajfer RA, Kilic A, Neviaser AS, et al. Enhancement of fracture healing in the rat, modulated by compounds that stimulate inducible nitric oxide synthase: Acceleration of fracture healing via inducible nitric oxide synthase. Bone Joint Res 2017; 6: 90-7. [Crossref]
26. R&D System. Wnt Receptors & Pathways. Available from: https://www.rndsystems.com/pathways/wnt-signaling-pathways-beta-catenin-dependent-wnt-signaling
27. Karner CM, Long F. Wnt signaling and cellular metabolism in osteoblasts. Cell Mol Life Sci 2017; 74: 1649-57. [Crossref]
28. Kato M, Patel MS, Levasseur R, et al. Cbfa1-independent decrease in osteoblast proliferation, osteopenia, and persistent embryonic eye vascularization in mice deficient in Lrp5, a Wnt coreceptor. J Cell Biol 2002; 157: 303-14. [Crossref]
29. Hojo H, Ohba S, Chung UI. Signaling pathways regulating the specification and differentiation of the osteoblast lineage. Regen Ther 2015; 1: 57-62. [Crossref]